

## Jump rate of the fcc vacancy in the short-memory–augmented-rate-theory approximation. II. Dynamical conversion coefficient and isotope-effect factor

M. Marchese, G. Jacucci,\* and C. P. Flynn

*Department of Physics and Materials Research Laboratory, University of Illinois at Urbana-Champaign, Urbana, Illinois 61801*

(Received 20 April 1987)

The framework of short-memory–augmented-rate theory is employed to partition the vacancy jump rate into two factors related, respectively, to the Vineyard theory and to corrections for multiple barrier crossings inherent in the dynamics. This paper treats the second of the factors using molecular dynamics to locate critical trajectories that lie on invariant manifolds of the dynamical systems, starting from states of motion in the saddle plane. For models of Ar, Cu, and Ag the errors of the Vineyard treatment are negligible at low temperature and contribute a rate reduction of only  $\sim 10\%$  at the melting temperature. These factors are, however, strongly mass dependent and give dominant contributions to the isotope effect. Our calculations reproduce the experimentally observed  $\kappa \approx 0.87$  near the melting temperature very well, and are similarly model insensitive;  $\kappa$  decreases nonlinearly from its harmonic value at  $T=0$  as the temperature is increased. Detailed examination of trajectories shows that the isotope effect is largely determined by the deformation of the manifolds caused by core repulsive forces. In effect, the isotope dependence derives mainly from infrequent energetic collisions that take place in jump events.

### I. INTRODUCTION

Classical statistical theory of diffusion jumps, as exemplified by Vineyard's<sup>1</sup> many-body formulation, has been unable to account for the isotope effects for diffusion observed in simple solids. The isotope-effect factor  $\kappa$  conveys the mass sensitivity of the jump rate  $R$  through the equation

$$\frac{R(M)}{R(M+dM)} = 1 + \kappa \frac{dM}{2M}, \quad (1)$$

so that  $K=1$  when  $R \sim M^{-1/2}$ , as is appropriate for an independent particle in thermal equilibrium. For fcc metals  $\kappa$  is typically 13% below unity,<sup>2</sup> and between 40% and 50% for bcc metals.<sup>2,3</sup> These are the consequences of cooperative motion by neighbors during the jump, which reduce the mass sensitivity. Regarded in this light the isotope effect offers a direct, and indeed the only, monitor of dynamics during the jump event itself. Calculations based on Vineyard's theory give reductions several times smaller than those observed.<sup>2</sup> It was suggested by Flynn<sup>4</sup> that the discrepancies must be temperature-dependent effects of anharmonicity that cause incorrect accounting for jump events. This was consistent with early molecular-dynamics simulations of a Lennard-Jones model for argon near its melting point by Bennett,<sup>5,6</sup> who computed for that model a mass sensitivity near the value actually observed in metals. A good deal more data<sup>7–9</sup> on various systems has accumulated since that time but no theoretical advances have occurred.

Because of its importance as a potential probe of jump dynamics, the isotope effect in diffusion warrants careful attention. Indeed, extensive experimental investigations were originally undertaken in the hope that the results could shed light on otherwise inaccessible phenomena

that take place in the jump process. At the same time, the fundamental question of precise criteria by which jump events can be identified has come to the forefront in our own research,<sup>10–12</sup> in that of Doll and Voter<sup>13–15</sup> on surface diffusion and, in a different context, in the rate processes exhibited by macromolecular systems.<sup>16</sup> One of the main results of the present paper is that the mass dependence of the jump criterion plays a critical role in determining the isotope effect in solid-state diffusion. By means of a precise formulation of the jump problem we are able to obtain an accurately predictive treatment of the isotope effect and to understand the physical causes of its hitherto unexplained behavior. These topics form the subject matter of the present paper.

This paper, the second of two, is concerned with the accurate description of jump processes within the short-memory–augmented-rate theory (SM-ART).<sup>11</sup> As described in the companion paper by De Lorenzi *et al.*<sup>17</sup> that precedes this, certain invariant manifolds in phase space divide the Hamiltonian flow over a potential barrier in a convenient way. Figure 1 shows schematically the stable ( $CS^+$ ) and unstable ( $CS^-$ ) center manifolds intersecting at the center manifold (CM) itself. For a crystal of  $N/3$  atoms CM is the  $(2N-2)$ -dimensional manifold of all trajectories that linger indefinitely on the barrier;  $CS^-$  is the  $(2N-1)$ -dimensional manifold obtained when CM is slightly disturbed so that this configuration decomposes, and  $CS^+$  is its time-reversed analog.  $CS^+$  and  $CS^-$  divide phase space into four sectors. Two of these pertain to flow over the barrier parallel to the reaction coordinate  $q_1$ . The important point is that each of the two contains all the flow in one sense, so that any surface  $\Sigma$  cutting the appropriate sector intersects all the flow. Consequently, the rate  $R$  at which jumps take place in one sense may be written as an integral of the

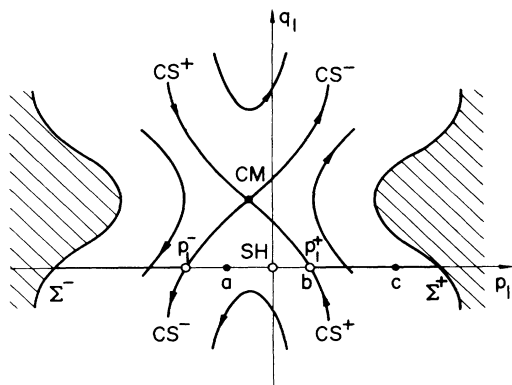


FIG. 1. Section of the tunnel in phase space connecting two equilibrium configurations  $A$  and  $B$ . The plane  $(q_1, p_1)$ , with  $q_1$  the reaction coordinate, is shown for a given choice of the remaining normal coordinate and momenta on  $SH$ . By definition (see text)  $SH$  is the origin while the intersection of this plane with the center manifold  $CM$  is the point specified by the crossing of the center stable ( $CS^+$ ) and unstable ( $CS^-$ ) manifolds;  $CS^+$  and  $CS^-$  partition the flow of trajectories with different fates. For a given state on  $SH$  a change of the normal momentum corresponds to displacement along  $p_1$ . Only trajectories with initial normal momentum  $p_1 > \max(p_1^-, p_1^+)$  belong to the successful jump flow from  $A$  to  $B$  [ $p_1 < \min(p_1^-, p_1^+)$  to the one from  $B$  to  $A$ ]. The full jump rate is obtained by integrating the flow through the surfaces  $\Sigma^\pm$ .

flow velocity  $\mathbf{X}$  over the surface  $\Sigma$ :

$$R = \frac{1}{Z_\Gamma} \int_\Sigma e^{-\beta H} \mathbf{X} \cdot d\mathbf{\Sigma}, \quad (2)$$

with  $H$  the Hamiltonian,  $\exp(-\beta H)$  the density distribution, and  $Z_\Gamma$  its normalization integral over the initial equilibrium configuration in phase space. When the surface  $\Sigma$  is chosen to extend from  $CM$  to regions of inaccessibly high energy, a more elegant formula, obtained by means of the Stokes theorem, displays the rate as a ratio between the partition function  $Z_\Gamma$  and that of the system constrained on the  $CM$ , namely  $Z_C$ :

$$R = \frac{Z_C}{\beta Z_\Gamma}. \quad (3)$$

This is the principal result of the SM-ART treatment of Toller *et al.*,<sup>11</sup> on which the work that follows is based.

We reiterate further, as in De Lorenzi *et al.*,<sup>17</sup> that it is often useful to work with a reference surface that has a simpler geometry than  $CM$  itself. This allows the total flow to be regarded as the flow with respect to the reference surface, together with a correction term that accommodates differences between the reference surface and the center manifold. A natural choice of reference is a “saddle hyperplane,”  $SH$ , namely the product space of a saddle plane and the momentum coordinate it contains; the plane itself can usefully be defined by diagonalizing the potential function about the saddle point of the potential barrier. Then the rate follows from Eq. (3) as

$$R = R_0 c, \quad (4)$$

with

$$R_0 = \frac{Z_{SH}}{\beta Z_\Gamma} \quad (5)$$

and

$$c = \frac{Z_C}{Z_{SH}}. \quad (6)$$

Or, alternatively, from Eq. (1), we may write

$$c = \frac{\beta}{Z_{SH}} \int_\Sigma e^{-\beta H} \mathbf{X} \cdot d\mathbf{\Sigma}. \quad (7)$$

Here  $Z_{SH}$  is the partition function of the system constrained on  $SH$ . The separation of these terms in Eq. (4) is the basis on which the present calculations are undertaken.

Equation (5) for  $R_0$  is essentially the Vineyard result<sup>1</sup> for the rate at which transitions take place through a planar saddle surface. Its precise evaluation for simple models of fcc solids is the task completed in the preceding paper. Our purpose in the present paper is to evaluate the dynamical “conversion coefficient”  $c$  to find the size of the error rate theory makes in counting the flux of transitions.

A point of special interest concerns the isotope effect which, from Eq. (1), is given by the expression

$$\kappa = -2 \frac{\partial \ln R}{\partial \ln M}. \quad (8)$$

Using Eq. (4) for  $R$ , we can factorize  $\kappa$  into two terms:

$$\kappa = -2 \frac{\partial \ln R_0}{\partial \ln M} - 2 \frac{\partial \ln c}{\partial \ln M} = \kappa_H - 2 \frac{\partial \ln c}{\partial \ln M}. \quad (9)$$

It has long been known<sup>4</sup> that the isotope-effect factor  $\kappa_H$ , for a barrier that is planar but otherwise arbitrarily anharmonic, is defined by the normal to the plane. For realistic models this gives predictions that are incorrect at high temperature, as first pointed out by Huntington *et al.*<sup>18</sup> In general the barrier is not planar,<sup>4,10</sup> however, and anharmonicity can bring mass-dependent terms into the conversion coefficient.<sup>4,10,12</sup> The consequent suggestion<sup>4</sup> that the experiments must probe the mass dependence of  $c$  is consistent also with the results of molecular dynamics simulation of Ar near its melting temperature.<sup>5,6</sup> Our interest in what follows therefore focuses on both the magnitude of  $c$  and its mass dependence.

The plan of the paper is as follows. In Sec. II we first address the topological structure of the invariant manifolds associated with the migration barrier, and then describe a numerical procedure for sampling the relevant manifolds to obtain the required correction factor. Section III presents the results of the calculations for models of Ar, Cu, and Ag. In the subsequent discussion of these data, and particularly their dependence on the interatomic potential, it is possible to identify without ambiguity the unexpected fact that energetic hard-core collisions play a major role in determining the isotope effect in diffusion. Section IV provides a brief summary of the results.

## II. APPLICATIONS OF THE THEORY

The framework outlined in Sec. I can be applied to the conversion coefficient in different ways and with various

levels of approximation. A principal purpose of this paper is to describe its exact, numerical evaluation within the SM-ART theory using the full interatomic potential. This is the main subject matter of Sec. II B. Section II A focuses on some analytical aspects that give useful insight into both the topology of the manifolds and the character of the trajectories around CM. In particular, one can calculate the partition functions of Eq. (3) for a truncated series expansion of the anharmonic potential energy and in this way obtain the jump properties as a power series in  $T$ . The first-order term in  $T$  has been determined and evaluated earlier<sup>11,12</sup> for particular model fcc systems. The results provide a theoretical framework on which the numerical methods may be based. A comparison among results from the various approaches in Sec. III gives new physical insight into the processes that determine the isotope effect.

#### A. Critical trajectories and the invariant manifolds

We are interested here in the trajectories available to a dynamical many-particle system near points at which the potential energy  $V$  possesses a simple saddle point  $P_0$ . The Hamiltonian of a crystal with  $N/3$  atoms can be expressed in terms of mass-weighted normal coordinates  $q_i$  of this saddle point, together with their canonically conjugate momenta  $p_i$ , as

$$H = \sum_{k=1}^N p_k^2 + V_0 - \frac{1}{2}\eta^2 q_1^2 + \frac{1}{2} \sum_{k=2}^N \omega_k^2 q_k^2 + V_a(q_1, \dots, q_N), \quad (10)$$

where  $V_a$  is an infinitesimal of third order containing all anharmonic parts of  $V$ . These normal coordinates  $q_i$  are obtained by an orthogonal transformation of the  $N$  mass-weighted atomic Cartesian coordinates,  $x_i M_i^{1/2}$ , with associated velocities  $\dot{x}_i$ ,  $i = 1, \dots, N$ , that diagonalize the dynamical matrix for the system at the saddle point  $P_0 \equiv (x_1^0, \dots, x_N^0)$ . Thus

$$\mathbf{D}_{rs} = (\mathbf{M}_r \mathbf{M}_s)^{-1/2} \left[ \frac{\partial^2 V}{\partial \mathbf{x}_r \partial \mathbf{x}_s} \right]_{P_0}, \quad (11)$$

such that

$$\mathbf{D}_{rs} \cdot \mathbf{a}_r^i = \varepsilon_i \mathbf{a}_s^i, \quad (12)$$

where  $\varepsilon_1 = -\eta^2$ ,  $\varepsilon_2 = \omega_2^2, \dots$ , and  $\varepsilon_N = \omega_N^2$  are the eigenvalues and  $\mathbf{a}_r^i$  the orthonormal eigenvectors which define the transformation

$$q_i = \sum_r \mathbf{M}_r^{1/2} \mathbf{a}_r^i \cdot (\mathbf{x}_r - \mathbf{x}_r^0). \quad (13)$$

We associate the position and velocities of the jumping atom with indices 1, 2, and 3 of the Cartesian coordinates. Further,  $q_1$  and  $p_1$  are the normal coordinate and momentum associated to the unstable mode at the saddle point; they define the “reaction coordinate” of the system.

For a dynamical system of this kind the center stable manifold  $\text{CS}^+$  and the center unstable manifold  $\text{CS}^-$  are given by equations of the kind:<sup>11</sup>

$$p_1^\pm = \mp \eta q_1 + F_\pm(q_1, q_2, \dots, q_N; p_2, \dots, p_N). \quad (14)$$

$\text{CS}^+$  and  $\text{CS}^-$  intersect in the center manifold CM described by the equations

$$\begin{aligned} q_1 &= f(q_2, \dots, q_N; p_2, \dots, p_N), \\ p_1 &= g(q_2, \dots, q_N; p_2, \dots, p_N). \end{aligned} \quad (15)$$

The functions  $F_\pm$ ,  $f$ , and  $g$  are defined for sufficiently small values of their arguments. Explicit analytical expressions for these functions, given in Ref. 11, and collected in the Appendix, are valid for a truncated power-series expansion of the anharmonic term  $V_a$  of the potential.

We wish to calculate the rate at which representative points pass through the surface  $\Sigma$  in Eq. (2). When this surface is defined by coordinates and conjugate momenta of a planar saddle surface, the behavior in the neighborhood of  $P_0$  is simplified. This “saddle hypersurface,” SH, defined by the equations

$$q_1 = 0, \quad p_1 = 0, \quad (16)$$

comprises a second  $(2N-2)$ -dimensional hypersurface analogous to the center manifold. The two coincide in general only for planar potential barriers. A given set of values for all the normal coordinates and momenta in SH are required to specify the Hamiltonian flow in the plane  $(q_1, p_1)$ . In this plane SH is a point that locates the origin. The center manifold is also a point but, being determined by Eq. (15), is in general different from SH. The forms of  $\text{CS}^+$  and  $\text{CS}^-$  remain determined by Eq. (14) and are represented in Fig. 1 as curves.

$\text{CS}^+$  and  $\text{CS}^-$  separate the flow paths through phase space of trajectories with different fates. This is the most important realization of the SM-ART treatment. All trajectories that cut the surface  $\Sigma$  that extends along the  $p_1$  axis from SH to remote regions, may cut it again later any number of times as the system evolves. However, only those trajectories that cross  $\Sigma$  in this section with  $p_1 > \max(p_1^-, p_1^+)$  belong to the flow of successful jumps from the equilibrium in configuration  $A$  to that in  $B$ , while for  $p_1 < \min(p_1^-, p_1^+)$  they belong instead to the net flow from  $B$  to  $A$ .

By means of exact numerical evaluations of the dynamics we have verified that the monotonic behavior indicated in Fig. 1 does indeed occur in real systems. In Fig. 2 we show the time evolution from an initial state on SH, projected along the reaction coordinate, for the three values of normal momentum  $p_1$  corresponding schematically to the points  $a$ ,  $b$ , and  $c$  of Fig. 1. Those momenta larger than  $p_1^+$ , e.g., point  $c$ , give trajectories leading directly to transitions from  $A$  to  $B$ ; upon reducing the normal momentum to  $p_1^+$  (point  $b$  in Fig. 1) there occurs a critical trajectory that lies on  $\text{CS}^+$ . Smaller momenta, e.g., point  $a$  lead to return jump trajectories that reverse their perpendicular momentum. Further reductions would result in a trajectory that originated at a prior time from oscillations near the barrier ( $\text{CS}^-$  at  $p_1^-$ ) and finally trajectories that correspond to jumps in the reverse direction. Note that the critical trajectories associated with  $\text{CS}^+$  and  $\text{CS}^-$  approach and

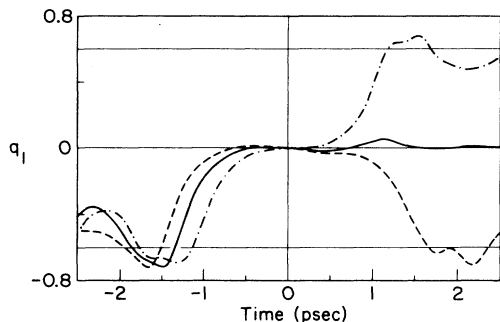


FIG. 2. Time evolution from an initial state on SH, projected along the reaction coordinate  $q_1$ , for a sequence of normal momenta,  $p_1$ , corresponding to points  $a$ ,  $b$ , and  $c$  in Fig. 1. The monotonic behavior predicted by the theory is confirmed. The  $CM^+$  trajectory (solid line, point  $b$  in Fig. 1) oscillates about the saddle plane in the forward time evolution. It separates the flow of return jumps having smaller normal momentum (dashed line,  $a$  in Fig. 1) from the flow of successful trajectories having larger normal momentum (dash-dotted line,  $c$  in Fig. 1).

linger indefinitely on top of the potential barrier, thus oscillating through the saddle plane. Similarly, all critical trajectories associated with the center manifold oscillate indefinitely about the saddle plane. For simple models of the anharmonic barrier, the nature and amplitude of such oscillations can be computed explicitly.<sup>19</sup> The fact that the critical trajectories do behave in this way plays a central role in their identification for the case of a general potential in Sec. II B.

The full jump rate is calculated by integrating the flow through the surface  $\Sigma^\pm$  of equations

$$q_1 = 0, \quad p_1 \geq \max(p_1^-, p_1^+) \quad (17)$$

for  $\Sigma^+$  and

$$q_1 = 0, \quad p_1 \leq \min(p_1^-, p_1^+) \quad (18)$$

for  $\Sigma^-$ . The dynamical conversion coefficient for the flow from  $A$  to  $B$  can then be evaluated by a thermal sampling of the hypersurface SH with analytical integration over all momenta larger than the critical one,  $p_c(P) \equiv p_1^+$ , be it positive or negative, for each sampling point  $P$  on SH; thus

$$c = \beta \left\langle \int_{p_c}^{+\infty} p_1 \exp(-\frac{1}{2}\beta p_1^2) dp_1 \right\rangle_{SH}. \quad (19)$$

An analogous expression holds for the flow in the opposite direction. Equation (19) is a central result of the present treatment. The topological structure of the manifolds provides a rigorous definition for the critical momenta  $p_c(P)$  as the momentum component perpendicular to SH required to place the trajectory on the center stable (or unstable) manifold for any given initial state on SH. The same structure then ensures that all larger momenta lead to complete jumps within the SM-ART formulation, much as assumed empirically in Bennett's calculation for a different definition of critical trajectory. As noted by Bennett,<sup>6</sup> the existence of a critical momentum allows sampling over the crossing momenta, still

used in other approaches,<sup>15</sup> to be replaced by a more efficient integral from  $p_c$  to infinity.

We now turn attention to a determination of the isotope-effect factor. It is important to realize that, within the SM-ART treatment, the conversion coefficient  $c$  for a particular jumping atom and that,  $c'$ , for a different isotopic mass constitute two entirely different problems. For both systems  $c$  is correctly represented by the ratio of partition functions in Eq. (6) or by the flux through a surface  $\Sigma^\pm$  as defined in Eq. (7). However, both the partition functions and the definition of  $\Sigma^\pm$  are complicated by the fact that the system with a different mass possesses a distinct saddle hypersurface  $SH'$  and center manifold  $CM'$  that are rotated and distorted with respect to those of the system with all masses equal. An accurate treatment of the isotope effect must therefore incorporate a correct description of the different jump conditions for the two systems.

For small changes in the mass of the jumping atom,  $M_1 \rightarrow M_1(1 + \delta)$ , the linear variation with  $\delta$  of the surfaces of interest can be calculated by use of first-order perturbation theory. In order to obtain insight into the computational problems this complication brings, it is useful to consider the initial example of a system represented by its anharmonic expansion carried through to terms of third order. For this system the isotopically modified manifolds can be expanded by perturbation theory in terms of the coefficients of the unmodified system. The algebraic details are collected in the Appendix. It turns out that Eq. (19), when written for this system, can be evaluated analytically to first order in  $T$ , and this approach naturally leads to the result reported in Ref. 12. Of greater interest here is the fact that Eq. (19) can also be obtained by using a numerical sample of states on SH and assigning to each the critical momentum determined by the corresponding analytical expression of Eq. (14). We find immediately that the expected difference is too small to be measured directly by separate sampling runs on the two systems, since  $c' - c \simeq 10^{-4}$  for  $\delta = 0.01$ . A determination of  $c' - c$  by means of separate numerical sampling on SH and  $SH'$  requires a number of sample points of the order of  $10^6$  to achieve an accuracy of 1% in  $\kappa$  for  $\delta = 0.01$ . Such large samplings are not feasible, so the determination of  $\kappa$  for a general potential, where the critical momentum  $p_c$  must be determined by numerical methods, requires a different approach.

To overcome this problem we have incorporated into our calculation a difference sampling method analogous to that proposed by Bennett<sup>6</sup> to compute the mass dependence of  $c$ . We investigate the mass dependence of the critical momenta  $p_c$  in a chosen sample of SH states of the  $M_1 = M$  system by establishing a one-to-one correspondence between each state  $P$  of SH,  $P = (x_1, \dots, x_N, \dot{x}_1, \dots, \dot{x}_N)$  and the equiprobable state of the  $M_1 = M'$  system, namely  $\tilde{P} = (x_1, \dots, x_N, \tilde{x}_1, \dots, \tilde{x}_N)$ . The transformation

$$\tilde{x}_i = \begin{cases} \dot{x}_i (M/M')^{1/2}, & i = 1, 2, 3 \\ \dot{x}_i, & i = 4, 5, \dots, N \end{cases} \quad (20)$$

ensures that the two states have the same statistical weight.

To employ this variance-reducing correspondence, one finds the critical normal momenta  $p_c(\bar{P})$  needed to place the trajectory of the new initial condition  $\bar{P}$  on  $CS^+$  (or  $CS^-$ ) for the  $M_1=M'$  system. The difference in conversion coefficient is then obtained as an average over states on SH of the integral between the two critical momenta, just as in Bennett's work. Application of this difference sampling method dramatically reduces the number of states in SH needed to obtain an accurate determination for  $\kappa$ . In the case described above (see the Appendix) the difference method requires about  $10^3$  states to obtain the same accuracy achieved by a sample 3 orders of magnitude larger, in the evaluation by separate runs.

### B. Sampling methods

For an arbitrary potential it is not, in general, possible to write down an analytical form for the CM. Numerical methods are therefore needed to locate CM,  $CS^-$ , and  $CS^+$ . For this purpose it is convenient to start from some specific locus in phase space. As explained in Sec. II, a natural choice that provides easy sampling of initial configurations is the saddle hyperplane SH.

The desired critical values of  $p_1$  and  $q_1$  are those for which the evolution of the representative point lies on the particular manifold of interest. These are determined by imposing the corresponding asymptotic behavior on the time evolution of the trajectory, namely, (a) the CM trajectory should oscillate indefinitely about the saddle plane; (b) the  $CS^+$  trajectory should oscillate about the saddle plane only for the forward time evolution for the trajectory; and (c) the time-reversed behavior should occur for the trajectory  $CS^-$ .

Any determination of CM trajectories themselves would require finding critical values for both  $q_1$  and  $p_1$ , and it would be necessary, in addition, to project the invariant measure of CM onto SH. We have therefore focused our effort instead on the determination of the critical momentum  $p_c$  required for an initial configuration on SH to obtain a trajectory on  $CS^+$  or  $CS^-$  and so to evaluate  $c$  by means of Eq. (19).

An implementation of these principles for any given structure and model potential requires several distinct steps. The saddle-point configuration  $P_0 \equiv (x_1^0, \dots, x_N^0)$  must first be determined and the potential diagonalized at  $P_0$  to yield eigenvalues and eigenvectors of Eq. (12) that define the saddle hypersurface SH. It is then necessary to sample representative points in phase space on the surface SH, and for each to iterate the evolution of trajectories for various normal momenta in order to locate the specific critical trajectory. The first step of the procedure has been carried out here using standard relaxation techniques such as those described in Ref. 10. The sampling on SH was performed by means of a molecular-dynamic (MD) run constrained to remain on SH. Details of the latter calculation are described in Sec. II B 1. The last step, namely the search for the critical trajectories, is the main topic of Sec. II B 2.

### 1. Sampling on a surface in phase space

Different methods have been widely used<sup>5,14,15,17</sup> to sample initial states on a surface in phase space for a given interatomic potential. In the present work we use an independent method to sample states on the saddle hyperplane. To maintain the dynamical system on SH we introduce an explicit dynamical constraint in the form of an external force  $\bar{\phi}$ , so that

$$q_1(t) = \sum_{i=1}^N a_i^1(x_i(t) - x_i^0) = 0 \quad (21)$$

for every  $t$ . From Eq. (21) it follows directly that also  $p_1(t)=0$  for every  $t$ . The force  $\bar{\phi}$ , applied in the direction of the constraint  $q_1 = (\{a_i^1\})$ , has Cartesian components

$$\phi_i = - \left[ \sum_{\alpha=1}^N a_{\alpha}^1 F_{\alpha}(t) \right] a_i^1, \quad (22)$$

where  $F_{\alpha}(t) = -(\partial V / \partial x_{\alpha})_{x(t)}$  is the usual force acting on particle  $\alpha$  in the absence of the constraint.

Because  $\bar{\phi}$  acts along the direction of the constraint it does no work on the system. Likewise, all linear momenta are conserved when the initial configuration is chosen on SH, the natural choice for it being  $P_0$ . By starting a molecular-dynamics run from  $P_0$  at a given temperature, subject to the Hamiltonian of the constrained system, we thus generate an ensemble of configurations on SH whose members are representative of configurations that would occur at thermal equilibrium for the unconstrained system of Hamiltonian  $H$ .

### 2. Determination of critical trajectories

Given an initial state on SH it is necessary to determine the critical value  $p_c$  of the perpendicular momentum. Our procedure uses a brief search of a generically broad interval of values of  $p_1$  to locate the transition from the flow of returns and to the flow of successful jumps. With a specific initial value  $p^0$  for the perpendicular momentum, chosen from within this interval (the natural choice being its arithmetic mean), the evolution of the system backward and forward in time is computed by MD for a period  $\tau = n\tau_0$  with  $\tau_0$  the time step. In this run we monitor the quantity

$$q_1(t; p^0) = \sum_{i=1}^N a_i^1(x_i(t; p^0) - x_i^0). \quad (23)$$

This projects the motion of the particles in the Cartesian space of the crystal onto the many-body reaction coordinate.

In addition, we calculate the time evolution of a perturbed trajectory,  $q_1(t; p^1)$ , for a slightly different initial value,  $p^1$ , of normal momentum. For small values of such perturbations the motion of the system falls in a linear-response regime where the magnitude of the mechanical response depends linearly on the strength of the applied perturbations.<sup>20,21</sup> Within this regime a general trajectory of normal momentum  $p$  can be obtained approximately as

$$q_1(t;p) \simeq q_1(t;p^0) + \frac{p-p^0}{p^1-p^0} \delta q_1(t;p^0, p^1), \quad (24)$$

where

$$\delta q_1(t;p^0, p^1) = q_1(t;p^1) - q_1(t;p^0). \quad (25)$$

In this way it is possible to study, within the linear-response approximation, the behavior of a family of trajectories, all originating from the same initial state on SH but corresponding to different values of the crossing momentum. An example of the resulting trajectories is given in Fig. 3.

The critical condition in which the system oscillates about the saddle plane can be expressed analytically by imposing an average of zero on the time integral of the reaction coordinate:

$$\int_0^\tau q_1(t;p) dt = 0 \quad (26)$$

for  $CS^+$  and

$$\int_{-\tau}^0 q_1(t;p) dt = 0 \quad (27)$$

for  $CS^-$ . We can now estimate the critical normal momentum within the linear-response approximation by use of Eqs. (24) and (27) or (28) as

$$p_c^\pm = p^0 + p^1 \Delta_\pm, \quad (28)$$

where

$$\Delta_+ = - \frac{\int_0^\tau q_1(t;p^0) dt}{\int_0^\tau \delta q_1(t;p^0, p^1) dt} \quad (29)$$

for  $CS^+$

$$\Delta_- = - \frac{\int_{-\tau}^0 q_1(t;p^0) dt}{\int_{-\tau}^0 \delta q_1(t;p^0, p^1) dt} \quad (30)$$

for  $CS^-$ . By iterating the procedure, using successive estimates of  $p_c$  as initial momenta  $p^0$ , the critical momen-

tum  $p_c$  can be obtained to any desired accuracy and for any interval  $\tau$  of integration. Such an estimate of  $p_c$  depends to some extent on the particular choice of  $\tau$ , but it must converge to a specific limit as  $\tau$  is increased. In the case described in the Appendix an analytical value of  $p_c$  can be obtained exactly. For the iterative method just described this example suggests that the convergence can be considered complete as soon as  $\tau$  approaches the characteristic time associated with the unstable mode frequency  $\eta$  ( $\sim 5-6$  Debye periods in the model studied, see Table I).

One further matter of computational significance warrants mention here. Rather than integrating  $q_1(t;p^0)$  and  $q_1(t;p^1)$  separately it has been possible, and computationally more economical, to solve an approximate differential equation for  $\delta q_1(t)$  itself, valid within the same linear-response approximation. The advantage lies in the fact that the expression for the gradient required in the integration of the equation of motion for  $\delta q_1(t)$  can be written at time  $t$  in terms of the second derivative of the potential function at the configuration of the unperturbed trajectory for the same time.<sup>21</sup> This result can be included at small cost in the same loop of the calculation of the gradient along the unperturbed trajectory. In practice the final search for  $p_c$  for any state on SH could be automated to require  $\sim 2.0$  min of CPU (central-processing-unit) time on an FPS264 processor.

It is evident that the values of critical momentum can be obtained for each state on SH. One of these (on  $CS^+$ ) is the critical momentum for jumps from  $A$  to  $B$ , and the other (on  $CS^-$ ) for jumps from  $B$  to  $A$ . Both can be used, as appropriate, in the evaluation of  $c$ . This halves the required sample of initial states on SH.

To evaluate the isotope-effect factor by means of the differential method described in Sec. II A, precisely the same procedure can be applied to find the critical momentum  $\bar{p}_c$  for the corresponding state in the system with a jumping atom of different mass. The critical momentum  $\bar{p}_c$  corresponds in principle to the component along the unstable mode  $q_1$ , required to place the trajectory on the different  $CS^+$  or  $CS^-$  of the new system, where it oscillates about the plane  $q_1' = 0$  rather than  $q_1 = 0$ . However, the computation effort is greatly reduced when the study is restricted to changes of critical momentum induced by a differential change in mass. In effect we confine attention to the mass derivative of  $c$

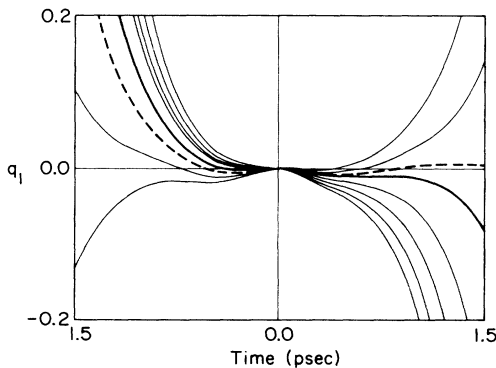


FIG. 3. Example of the numerical procedure used to determine the critical momentum  $p_c$  required to place the trajectory on  $CS^+$  for any initial state on SH. The thick line is an initial guess at the critical momentum; fine lines are trajectories computed in the linear-response approximation for different values of  $p_1$ . The dashed line is the improved estimate of the  $CS^+$  trajectory.

TABLE I. Numerical example of the dependence of the computed values  $p_c(P)$  and  $p_c(\bar{P})$  at  $T=0.1T_m$ ,  $\delta=0.01$  [ $T_m=0.67\epsilon$ ; see De Lorenzi *et al.* (Ref. 17)] on the time of integration  $\tau/\tau_\eta$  ( $\tau_\eta=2.2$  psec), for a state  $P$  on SH of the model potential described in the Appendix. Analytical values of  $p_c$  and  $\bar{p}_c$  reported in the last row for comparison correspond to an infinite integration time.

$\tau/\tau_\eta$	$p_c(P)$	$p_c(\bar{P})$
0.40	0.050 644 563 4	0.050 038 766 3
0.80	0.058 150 133 3	0.057 494 734 1
1.20	0.058 152 309 0	0.057 508 694 4
$\infty$	0.058 152 327 7	0.057 508 710 2

at  $M_1 = M$ . It is important to observe that a trajectory that lingers on the top of the barrier does so however one defines the plane of oscillation. In fact, the new reaction coordinate  $q'_1 = q_1 + \delta \sum_j \alpha_{1j} q_j$  (see the Appendix) oscillates with a phase that depends on  $q(t)$  so that any individual  $q_i$  appears with an essentially random phase. As it enters  $q'_1$  linearly it thus vanishes from  $\langle q'_i \rangle$ . The criteria  $\langle q_i \rangle = 0$  and  $\langle q'_i \rangle = 0$  therefore lead to identical results for  $\bar{p}_c$ .

A second useful point is that, when the mass change is small, an excellent guess for  $\bar{p}_c$  is given by the value of  $p_c$  previously calculated for the corresponding state for  $M_1 = M$ , so that fewer iterations are needed to converge on the new critical value. The same program, modified only to treat the different dynamics associated with the new mass, gave the value of  $\bar{p}_c$  for the new state in less than 1 min of CPU time.

As examples Table II gives average values of  $c$  and  $\kappa$  at two different temperatures, obtained by the procedures just described, for the anharmonic expansion for Lennard-Jones (LJ) argon (see the Appendix) for comparison with the exact values for the same model evaluated analytically. There is excellent agreement between the two sets of data. These results provide a check on the procedures that are the basis for our subsequent exploration of conversion coefficients and isotope-effect factors for full interatomic forces. A summary of these latter calculations is provided in Sec. III.

### III. NUMERICAL RESULTS

Our calculations follow earlier simulation of vacancy jumps by Bennett in which the conversion coefficient and nonharmonic isotope-effect factor were first computed for a Lennard-Jones fcc crystal near its melting point. Our work expands on these efforts in two directions. First, as explained above, we base our calculations on the SM-ART treatment in order to establish a rigorous theoretical framework for the results. Second, we have pursued these goals with much improved statistical precision. As will be apparent in what follows, the more accurate results allow new insight into the temperature, volume, and model potential dependences of the properties, and hence to a specific understanding of the anharmonic effects and their origins in atomic interactions.

As in the original SM-ART formulation by Toller *et al.*<sup>11</sup> our numerical results focus on particular models of Ar, Cu, and Ag. Details of the Lennard-Jones potential employed for Ar and the Morse potential used for Cu and Ag are provided in the paper by De Lorenzi *et al.*<sup>17</sup> that immediately precedes the present work, to which the reader is referred. For reasons of computational effort our calculations were confined to a 32-site fcc cluster with periodic boundary conditions, and with all sites but one occupied by atoms interacting through the chosen force laws. Details of the potential range and boundary effects are discussed by De Lorenzi *et al.*<sup>17</sup> It is our experience that these questions have little material effect on the conclusions drawn from the results reported in what follows.

In order to obtain a broad understanding of the pro-

cesses under study we have completed model calculations at several levels of approximation. These include a full numerical investigation in which the real manifolds are sampled for the complete force law in order to obtain a complete and accurate determination of  $c$  and  $\kappa$ , together with their temperature and volume dependences. We refer to these calculations below as pertaining to the exact model. In addition, it has been valuable to examine the analogous results obtained by sampling methods when the exact model potential is replaced by a smoothed model that contains only the low-order terms of a truncated anharmonic expansion of the potential energy about the saddle-point configuration, as described in the Appendix. This system differs from the exact model mainly by the elimination of hard-core repulsive energy as two atoms approach each other closely. We refer to these results as deriving from sampling for a model with a truncated anharmonic expansion. Finally, from earlier work, we have available analytical results that express  $c$  and  $\kappa$  by a low-temperature expansion in powers of  $T$ , that also depends on an anharmonic expansion of the potential energy in the vicinity of the saddle-point configuration. These results are referred to as deriving from an analytical treatment of the anharmonic expansion.

Results for the conversion coefficient  $c$  and isotope-effect factor  $\kappa$  as functions of temperature for these three different calculations are given for fcc Ar in the upper panels of Fig. 4. Each point in Fig. 4 required a sample containing 400 independent configurations. The error bars, where visible, indicate that the final uncertainties are kept below 1% in both  $c$  and  $\kappa$ . Figure 4, together with Table II, shows that the analytical and numerical

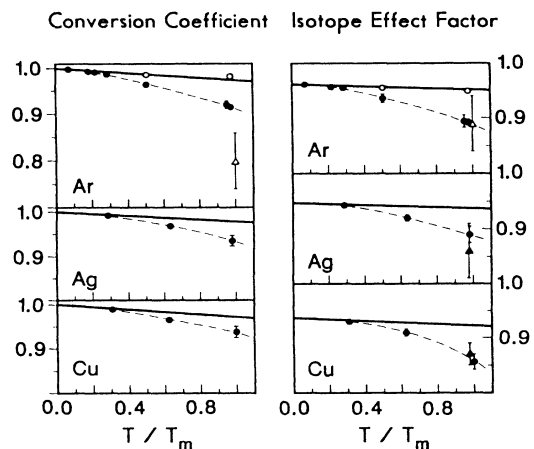


FIG. 4. The conversion coefficient  $c$  and the isotope-effect factor  $\kappa$  as functions of  $T/T_m$  for the exact models of fcc Ar, Ag, and Cu are shown by solid circles and connected by a dashed line as a guide to the eye. Analytical results for the anharmonic expansion (Ref. 11) (solid line) and sampling results for the same potential give identical results for argon (open circles). Points ( $\Delta$ ) are values for  $c$  and  $\kappa$  computed by Bennett (Ref. 6) for Ar. Points ( $\blacktriangle$ ) are experimental measurements of  $\kappa$  from Peterson (Ref. 2); they agree with the exact models but not with the anharmonic expansion (see text).

TABLE II. Values of the conversion coefficient and isotope-effect factor at two temperatures for the model potential of the Appendix, as computed by the numerical procedure (fourth and sixth columns) together with the corresponding analytical values (Refs. 11 and 12) (third and fifth columns). The second column gives the number of states on SH used in the sampling.

$T/T_m$	$N$	$c$		$K$	
		Analytical	Numerical	Analytical	Numerical
0.50	400	0.9868	$0.9855 \pm 0.0016$	0.9558	$0.9545 \pm 0.0028$
1.00	400	0.9790	$0.9801 \pm 0.0020$	0.9513	$0.9482 \pm 0.0038$

results for the anharmonic expansions are in essentially exact agreement. This verifies that each method provides an adequate account of the dynamical behavior for the smoothed potential. A startling discrepancy nevertheless exists between the exact model and the results for the truncated expansion. Whereas the latter exhibit only a weak linear temperature dependence in both  $c$  and  $\kappa$ , the results for the realistic potential exhibit a nonlinear dependence on  $T$  and a much larger deviation from unity. These effects are far outside the statistical uncertainties and must be regarded as firmly established by our calculation.

The lower panels of Fig. 4 compare the exact models with predictions for the truncated potentials of Cu and Ag. In both cases, and for both  $c$  and  $\kappa$ , there is a remarkable similarity between the calculated results and those for Ar. The calculated isotope effects obtained from the exact model for Cu and Ag agree well with the measured values, shown as solid triangles. More globally, all three exact calculations give an isotope effect near the melting temperature ( $T_m$ ) of about 0.87, which is typical of the values more generally observed for fcc lattices. It seems apparent that the fcc lattice produces an isotope effect that is decreased by anharmonicity from the harmonic value<sup>11</sup> at low temperature to this fairly reproducible value near  $T_m$ , much as suggested earlier by Flynn.<sup>4</sup>

Analogous comments describe the calculated conversion coefficients. In each case the exact values decrease from unity at  $T=0$  to about 0.9 at  $T_m$ , and with functional forms that have a remarkably similar dependence on  $T/T_m$ . The corrections to rate theory these results require are rather modest, and amount to about 10% at melting. This confirms earlier theoretical estimates<sup>4,10,11,22,23</sup> for dynamical corrections to rate theory in fcc systems. We note that some discrepancy exists between our LJ value of  $c$  near  $T_m$  and that given earlier by Bennett.<sup>6</sup> We believe that the differences are likely to be statistical in origin, rather than arising from differences of principle or from the different criteria employed for the critical trajectories. Numerical estimates of dynamical corrections to rate theory for surface diffusion reported by Voter and Doll<sup>15,24</sup> also amount to about 10% in the range of temperatures experimentally observed. Thus conventional rate theory as formulated by Vineyard gives an excellent approximation to the true jump rate for these systems with high barriers to atomic migration. However, this situation is not general and breakdown may occur for interstitial migration or even

for vacancy migration in softer materials with lower potential barriers.

The precision with which our calculations distinguish the consequences of different interatomic potentials affords a unique opportunity to explore the physical processes that determine the isotope effect and conversion coefficient of realistically anharmonic crystals. For this purpose the isotope effect is the main focus of attention. In practice, the conversion coefficient itself cannot be measured, and amounts at most to 10% changes of a rate that varies exponentially with temperature by many orders of magnitude over the experimentally accessible range. In contrast, the isotope effect—mainly the mass dependence of the conversion factor—is experimentally accessible to 1% precision in favorable cases, given the diffusion mechanism, and remains the only available monitor of dynamical processes that take place during the diffusion jump. Our discussion of the detailed dynamics is therefore restricted to the isotope-effect factor  $\kappa$ .

The results in Fig. 4 suggest that closed-shell repulsion may be the critical ingredient in determining the observed isotope effects. One may reason that the anharmonic expansions all give similar but *incorrect* isotope effects, and that by construction they differ from the exact results, which all give similar and *correct* behavior, mainly by the omission of the hard-core forces. Therefore our purpose in what follows is to investigate the actual role of atomic size in general, and core repulsion in particular, in determining the isotope effect. To this end two distinct series of calculations have been made. The first involves the character of the trajectories and the second an alternative simplified simulation of atomic size.

We have followed trajectories of the exact and truncated systems from the same initial configurations, through the critical condition at which a jump does or does not occur, to identify the differences caused by the hard core of the exact potential. In general the trajectories of the two systems are remarkably alike. We find, however, that large departures occur in a small, temperature-dependent fraction of the trajectories. It turns out that these differences invariably originate at a point on the trajectory at which the diffusing atom undergoes a vigorous collision with one of its neighbors, such that the hard-core forces of the exact potential exert a significant effect and thus modify the subsequent evolution of the system. Moreover, we find that it is precisely this same subset of trajectories that have large



changes of critical momentum, and that contribute the overwhelming portion of the calculated change of isotope effect. These results therefore establish beyond doubt that the observed isotope effects are determined in large part by infrequent, highly anharmonic processes that lie completely beyond the scope of available analytical theories. This is the reason the observed behavior has remained unexplained. From our present perspective we may observe that the repulsive core of the potential has a specific effect in deforming the center manifold, and to an extent that is strongly mass dependent. It is these changes that the isotope effect monitors.

Our conclusions are supported by the results of trajectory calculations summarized in Fig. 5. The figure shows, trajectory by trajectory, how the normalized fractional deviation  $\Delta c$  of the conversion coefficient from its truncated-potential value depends on the dynamics of the particles in the vicinity of the migrating atom. To obtain this concise information we have made use of the fact that motion along small principal radii of saddle-surface curvature (i.e., large curvatures) corresponds to relative moments localized at the migrating atom and its neighbors. These geometrical features of the saddle surface are described in an earlier report<sup>10</sup> and will not be reviewed here. For the present purpose we merely employ the components of the motion along these specific directions in configurational space to project out energetic collisions that involve the jumping atom. In Fig. 5 the fractional change of conversion coefficient is shown as a function of  $Q = \sum_i \epsilon_i / \rho_i^2$  for the trajectory. Here  $\epsilon_i$  is the summed kinetic and potential energy owing to motion and displacements of the initial state along direction  $i$  (the harmonic value was used for the potential), and  $\rho_i$  is the principal radius  $i$  of saddle-surface curva-

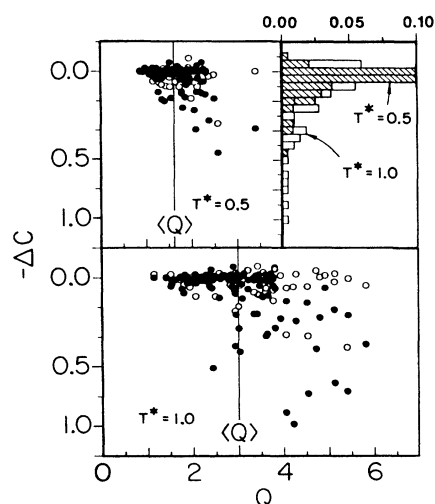


FIG. 5. Fractional change of  $c$  between the exact and truncated potential results for each sampled configuration on SH, shown as a function of  $Q = \sum_i \epsilon_i / \rho_i^2$  (see text) at  $T = 0.5T_m$  and  $T = 1.0T_m$  ( $T_m = 0.67\epsilon$ ; see paper I). The faint lines indicate the mean value of  $Q$  for the sample. The inset histograms show the long, temperature-dependent tails of the distributions that result from energetic hard-core collisions for these two temperatures.

ture.  $Q$  is therefore a monitor of the behavior of energetic relative motion between the migrating atom and its neighbors. The behavior of time-reversed trajectories from the same initial state is also indicated in Fig. 5.

It is strikingly evident in Fig. 5 that the great majority of trajectories, and particularly those with  $Q$  small, have  $\Delta c \approx 0$ . Particularly for  $Q$  large, however, there is a significant fraction of trajectories with  $\Delta c$  large and negative. This fraction decreases at lower temperatures, as shown at top left in Fig. 5 and as indicated by the histograms. The identifications of these changes with energetic local collisions is further confirmed by the fact that trajectories with initial velocities so directed as to *increase* the initial displacements (solid points) invariably have larger deviations than their time-reversed analog (open circles) that have the same value of  $Q$  but in which the velocity is directed to decrease the displacements. The velocity reversal gives a longer time interval for the energy to disperse before a collision. All these results therefore point clearly to the way in which the changes of  $c$  arise from local strong collisions during a potential jump event.

With these results in mind we have performed additional calculations to identify the explicit effects of atomic size. Rigid cores of radius  $\sigma'$  were superposed on the truncated expansion for the Lennard-Jones case in order to tune the potential from the smooth form to a more realistic form with a variable core size obtained by changing  $\sigma'$ . The results provide a convincing confirmation of the core effect discussed above. As seen in Fig. 6, both  $c$  and  $\kappa$  near  $T_m$  remain close to their truncated-potential values until  $\sigma'$  approaches  $0.9\sigma$ , with

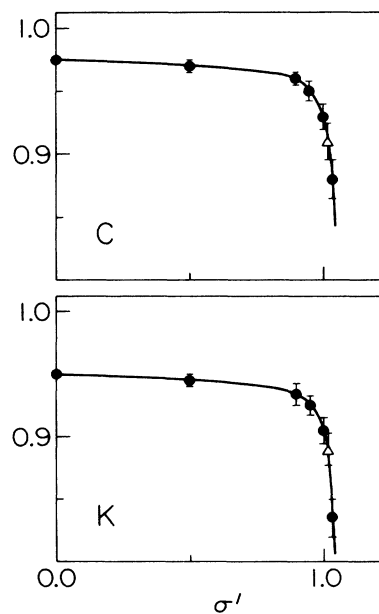


FIG. 6. Conversion coefficient and isotope-effect factor at fixed temperature  $T = T_m$  and density  $\rho = \rho_m$  when the anharmonic expansion is augmented by a hard-core interatomic repulsion of varying diameter  $\sigma'$  (in units of  $\sigma$ ,  $\sigma$  being the usual Lennard-Jones diameter). Points ( $\Delta$ ) are results for the ordinary Lennard-Jones potential at  $\sigma'_{LJ} = 1.02$ .

$\sigma$  the Lennard-Jones radius, at which point marked reductions both of  $c$  and  $\kappa$  begin. For this temperature the appropriate hard-core radius of the model is  $1.02\sigma$ , obtained by extrapolating Verlet's liquid-state data.<sup>25</sup> When  $\sigma'$  is increased to  $1.02\sigma$ , the values  $c=0.90$  and  $\kappa=0.89$  are obtained from our hard-core calculations. Thus the superposition of an appropriate atomic size on the smooth potential brings the properties back into excellent agreement with the exact results of Fig. 4. The insensitivity of these phenomena to all except the core forces and size is once more clearly emphasized. It is worth noting in this connection that for  $\sigma'=1.06\sigma$  the saddle point itself is occluded by rigid-core overlap. The seriousness of this core radius constraint on saddle-surface dynamics has not been given sufficient attention in prior research.

If the jump characteristics depend so strongly on the core radius then there must exist a complementary sensitivity to the crystal density and hence pressure. We have carried through the relevant calculations to confirm that this is the case. Because the compressibility of solids is small, however, the resulting effects on  $c$  and  $\kappa$  turn out significant but not large in size. A simple estimate comes from the hard-core model and the results in Fig. 6. We may write

$$V \frac{\partial c}{\partial V} = -\sigma' \left[ \frac{\partial c}{\partial \sigma'} \right]_{a_0} \left[ \frac{V_0}{V} \right]^{1/3}, \quad (31)$$

$$V \frac{\partial \kappa}{\partial V} = -\sigma' \left[ \frac{\partial \kappa}{\partial \sigma'} \right]_{a_0} \left[ \frac{V_0}{V} \right]^{1/3}, \quad (32)$$

whence, from the derivatives in Fig. 6,

$$V \frac{\partial c}{\partial V} = 0.46 \pm 0.03 \quad (33)$$

and

$$V \frac{\partial \kappa}{\partial V} = 0.6 \pm 0.1 \quad (34)$$

near  $T_m$ . These results show that the fractional changes of  $c$  and  $\kappa$  have the same order of magnitude as the volume changes that cause them at the equilibrium density near melting. Accordingly, the pressures required to produce measurable isotope-effect changes are not readily achieved. Nevertheless, the calculated temperature and volume dependences of the isotope effect are predictions of the theory that remain for experiment to explore.

For Ar we have pursued these questions one step further by means of explicit calculations of  $c$  and  $\kappa$  for the exact model system. Table III compares the results for three lattice spacings with the estimates from the hard-core calculations. The exact and hard-core results for the changes of  $c$  and  $\kappa$  agree to within their statistical uncertainties. Thus Table III provides a final confirmation that these properties are largely determined by the dynamics of hard-core collisions.

#### IV. SUMMARY

We have shown in this paper that molecular dynamics may be used to incorporate exact dynamical behavior into an investigation of vacancy jump processes in solids. This permits a complete and accurate evaluation of the atomic jump rate within the SM-ART treatment. To the extent that long-term correlations appear negligible we obtain an exact prediction of the classical jump rate. In conjunction with the calculations of saddle-plane properties by De Lorenzi *et al.*<sup>17</sup> described in the preceding paper our results offer, for the first time, jump rate predictions for solids with 1% accuracy directly from the atomic masses and interatomic potential. For the fcc vacancy diffusion discussed here, the many-body rate theory of Vineyard is itself an excellent first approximation; it overestimates the jump rate by only 10% at the melting temperature and the error falls to zero as  $T \rightarrow 0$ .

We have used the available computational precision to study the dependence of conversion coefficient and isotope-effect factors for these systems on the details of their interatomic potentials. The isotope effects calculated for the realistic potentials agree very well with experimental results for fcc metals near the melting temperature, and the calculations give very similar values of  $\kappa$  from one system to the next, just as is observed. It has been possible to demonstrate unambiguously that the values of  $c$  and  $\kappa$  are mainly determined by the core repulsive forces, through infrequent hard-core collisions undergone by the migrating atom during the jump events. This accounts for the remarkable similarities among the conversion coefficients and isotope-effect factors of different model fcc solids when shown in reduced form as a function of  $T/T_m$ . The calculations predict a nonlinear decrease of  $\kappa$  from its harmonic value at  $T=0$ , and also a significant volume dependence of  $\kappa$ , both deriving from these hard-core effects.

TABLE III. Comparison between predicted [Eqs. (33) and (34)] and computed values for  $c$  and  $K$  for the model of Ar at three different densities and at fixed temperature  $T = T_m$ .

$a/\sigma$	$\Delta V/V$	$\rho/\rho_0$	$c$ Predicted	$c$ Computed	$K$ Predicted	$K$ Computed
1.6403	0.00	1.00		$0.905 \pm 0.005$		$0.891 \pm 0.006$
1.5771	-0.05	1.05	$0.890 \pm 0.010$	$0.885 \pm 0.010$	$0.865 \pm 0.016$	$0.871 \pm 0.015$
1.5489	-0.10	1.10	$0.872 \pm 0.010$	$0.874 \pm 0.015$	$0.830 \pm 0.016$	$0.848 \pm 0.018$

## ACKNOWLEDGMENTS

We have benefited from discussion with M. Toller and from the advice and assistance of G. De Lorenzi. This research was supported in part through the University of Illinois Materials Research Laboratory, with funds provided by the National Science Foundation, under Grant No. DMR-83-16981. One of us (G.J.) thanks the University of Illinois National Center for Supercomputing Applications for support during a visit.

## APPENDIX

Our aim here is to introduce a useful model potential that we can use both for explicit analytical calculations and for testing the numerical procedures described in Sec. II B. In particular, we are interested in explicit expression for the center manifold (CM) and the center stable and unstable manifolds ( $CS^+$  and  $CS^-$ ) for this system, as well as their mass dependences. For this purpose we use a number of results found in earlier work<sup>10-12</sup> to which reference should be made for details.

The chosen potential is obtained from a general potential at a single saddle point  $P_0$ , such as that in Eq. (10), when the term contribution  $V_a$  is expressed in a power-series expansion in the displacements from  $P_0$ :

$$V_a = \frac{1}{6} \sum_{i,j,k=1}^N d_{ijk} q_i q_j q_k + \frac{1}{24} \sum_{i,j,k,r=1}^N e_{ijk r} q_i q_j q_k q_r + \cdots \quad (A1)$$

The truncation leaves an anharmonic model potential which contains some of the anharmonic properties of interest in diffusion problems, including a curved saddle surface and some anharmonic characteristics of CM,  $CS^+$ , and  $CS^-$ , but which can still be treated analytically. The coefficients that appear in Eq. (A1) can be determined for a given interatomic potential, as in Refs. 10 and 11 for the Lennard-Jones potential, and the analytical results then used to identify the effects of higher anharmonic terms.

Here we employ the power series truncated after terms of third order in the  $q_i$  so that  $V_a$  contains only coefficients of the kind

$$d_{ijk} = \left[ \frac{\partial^3 V}{\partial q_i \partial q_j \partial q_k} \right]_{P_0} \quad (A2)$$

Then Eqs. (15) and (14) for CM,  $CS^+$ , and  $CS^-$  can be developed as power-series expansions in the  $q_i$ :<sup>11</sup>

$$f = \frac{1}{2} \sum_{i,k=2}^N u_{ij} q_i q_k + \frac{1}{2} \sum_{i,k=2}^N v_{ik} p_i p_k + \cdots, \quad (A3)$$

$$g = \sum_{i,k=2}^N w_{ik} q_i p_k + \cdots, \quad (A4)$$

$$F_{\pm} = \pm \frac{1}{6\eta} d_{111} q_1^2 \pm \left[ \sum_{k=2}^N d_{11k} \frac{2\eta q_k \pm p_k}{4\eta^2 + \epsilon_k} \right] \times q_1 \pm \eta f + g + \cdots, \quad (A5)$$

where the coefficients  $u_{ik}$ ,  $v_{ik}$ , and  $w_{ik}$ , fixed by the eigenvalues  $\epsilon_i$  (note that  $\epsilon_1 = -\eta^2$ ) and the third-order

coefficients  $d_{ijk}$  of the potential  $V$  at  $P_0$  are

$$u_{ik} = 2h_{ik} d_{1ik}, \quad (A6)$$

$$v_{ik} = (\eta^2 + \epsilon_i + \epsilon_k) h_{ik} d_{1ik}, \quad (A7)$$

$$w_{ik} = (\eta^2 - \epsilon_i + \epsilon_k) h_{ik} d_{1ik}, \quad (A8)$$

$$h_{ik} = [\eta^2 + \epsilon_i + \epsilon_k + 2(\epsilon_i \epsilon_k)^{1/2}]^{-1} \times [\eta^2 + \epsilon_i + \epsilon_k - 2(\epsilon_i \epsilon_k)^{1/2}]^{-1}. \quad (A9)$$

The critical momentum that displaces the initial trajectory  $(0, q_2, \dots, q_N, 0, p_2, \dots, p_N)$  on SH onto  $CM^+$  or  $CM^-$  is

$$p_c^{\pm} = \pm \eta f + g. \quad (A10)$$

This result can be used in Eq. (19) and the integration on SH carried out either analytically or numerically to yield the result for the conversion coefficient to first order in  $T$  given in Ref. 11.

When the mass  $M_1$  of the jumping atom is changed, the system with changed mass has new orthonormal eigenvectors that are rotated with respect to the old ones. Moreover, the two systems possess two distinct CM,  $CS^+$ , and  $CS^-$ . For small changes in mass,  $M_1 \rightarrow M_1(1 + 2\delta)$ , the linear variation with  $\delta$  of the quantities that enter the equations for  $CS^+$  and  $CS^-$  can be evaluated by first-order perturbation theory. The calculation proceeds by first expressing the new coordinates, momenta, eigenvalues, eigenvectors, and third-order coefficients (identified here by primes) in terms of the old ones:<sup>12</sup>

$$q'_i = q_i + \delta Q_i, \quad Q_i = \sum_{j=1}^N \alpha_{ij} q_j, \quad (A11)$$

$$p'_i = p_i + \delta P_i, \quad P_i = \sum_{j=1}^N \alpha_{ij} p_j, \quad (A12)$$

$$\epsilon'_i = \epsilon_i + \delta E_i, \quad E_i = -2\epsilon_i \alpha_{ii}, \quad (A13)$$

$$d'_{ijk} = d_{ijk} + \delta D_{ijk}, \quad D_{ijk} = \sum_{r=1}^N (\alpha_{ri} d_{rjk} + \alpha_{rj} d_{irk} + \alpha_{rk} d_{ijr}). \quad (A14)$$

Here

$$\delta = d \ln(M_1)^{1/2} = \frac{dM_1}{2M_1}, \quad (A15)$$

and

$$\alpha_{ij} = (\mathbf{a}_1^i \cdot \mathbf{a}_1^j) \frac{2\epsilon_j}{\epsilon_j - \epsilon_i}, \quad (i \neq j) \text{ and } \alpha_{ii} = \mathbf{a}_1^i \cdot \mathbf{a}_1^i. \quad (A16)$$

From the above results, after a long but simple calculation, one can obtain all the coefficients that enter in the expression of the  $CS^+$  and  $CS^-$ :

$$u'_{ik} = u_{ik} + \delta U_{ik}, \quad (A17)$$

$$v'_{ik} = v_{ik} + \delta V_{ik}, \quad (A18)$$

$$w'_{ik} = w_{ik} + \delta W_{ik}, \quad (A19)$$

where

$$U_{ik} = u_{ik} \left[ A_{ik} - 2 \frac{t'_{ik}}{t_{ik}} \right] - \frac{t_{ik} D_{1ik}}{t_{ik}^2 - 4\epsilon_i \epsilon_k}, \quad (\text{A20})$$

$$V_{ik} = v_{ik} A_{ik} - \frac{2D_{1ik}}{t_{ik}^2 - 4\epsilon_i \epsilon_k}, \quad (\text{A21})$$

$$W_{ik} = U_{ik} - \epsilon_i V_{ik} + 2\epsilon_i v_{ik} \alpha_{ii}, \quad (\text{A22})$$

and with

$$A_{ik} = \frac{4t_{ik} t'_{ik} - 8\epsilon_i \epsilon_k (\alpha_{ii}^2 + \alpha_{kk}^2)}{t_{ik}^2 - 4\epsilon_i \epsilon_k}, \quad (\text{A23})$$

$$t_{ik} = \eta^2 + \epsilon_i + \epsilon_k, \quad (\text{A24})$$

$$t'_{ik} = \eta^2 \alpha_{11} + \epsilon_i \alpha_{ii} + \epsilon_k \alpha_{kk}. \quad (\text{A25})$$

The critical perpendicular momentum  $p'_c$  along the new unstable mode  $q'_1$  can thus be written by analogy with Eq. (A10), for any configuration  $(q'_1, q'_2, \dots, q'_N; p'_1, p'_2, \dots, p'_N)$  of the new system, as

$$p'_c = \mp \eta' q'_1 + F_{\pm}(q'_1, q'_2, \dots, q'_N; p'_2, \dots, p'_N). \quad (\text{A26})$$

Equation (A26) can now be used to calculate the conversion coefficient  $c'$  for the system with the different mass by means of the equivalent of Eq. (19) for this new system.

In order to apply these results in the difference method required to compute the isotope effect we need to specialize the result of Eq. (A26) by explicitly introducing the correspondence between the state  $P \equiv (0, q_2, \dots, q_N; 0, p_2, \dots, p_N)$  of the system with all masses equal, and the equiprobable state  $\bar{P} \equiv (\bar{q}'_1, \bar{q}'_2, \dots, \bar{q}'_N; \bar{p}'_1, \bar{p}'_2, \dots, \bar{p}'_N)$  of the system with the mass of the jumping atom changed. We note here that the point  $\bar{P}$  does not lie on the new saddle surface  $\text{SH}'$ , but rather on the old  $\text{SH}$ . However, it is still possible by means of Eq. (A26) to find its critical momentum (note that one cannot now disregard terms involving the  $q'_1$  coordinate). The correspondence given in the text in Cartesian coordinates can be expressed in the normal coordinate of the new system as

$$\begin{aligned} \bar{q}'_i &= q'_i, \\ \bar{p}'_i &= p'_i - \delta \Delta'_i, \quad \Delta'_i = \sum_{j=1}^N (\mathbf{a}_1^i \cdot \mathbf{a}_1^j) p'_j, \end{aligned} \quad (\text{A27})$$

where tildes are used to denote the component of  $\bar{P}$ . By means of Eqs. (A11), (A12), and (A27) we obtain the new state  $\bar{P}$  in terms of the old coordinates and momenta, to the lowest order in  $\delta$ :

$$\begin{aligned} \bar{q}_i &= q_i + \delta Q_i, \\ \bar{p}_i &= p_i + \delta P_i - \delta \Delta_i, \quad \Delta_i = \sum_{j=1}^N (\mathbf{a}_1^i \cdot \mathbf{a}_1^j) p_j. \end{aligned} \quad (\text{A28})$$

By substituting Eq. (A27) into Eq. (A26) the critical momentum along the new unstable mode  $\bar{p}'_c$  can now be evaluated for every  $\bar{P}$  in terms of the old coordinates and momenta. For our difference calculation we are interested, instead, in the component of the new critical momentum along the old unstable mode  $q_1$  that is given to first order in the mass change by the equation

$$\bar{p}_c = \bar{p}'_c - \delta P_1. \quad (\text{A29})$$

On applying the above relation to Eq. (A26) and by repeated use of Eqs. (A11)–(A19) we finally obtain the expression for the corresponding critical momentum:

$$\bar{p}_c = p_c - \delta A + \delta B, \quad (\text{A30})$$

with

$$A = p_c \alpha_{11} \pm \frac{1}{2} \sum_{i,k=2}^N (v_{ik} p_i \Delta_k + v_{ik} \Delta_i p_k) + \sum_{i,k=2}^N w_{ik} q_i \Delta_k, \quad (\text{A31})$$

$$\begin{aligned} B &= \mp \eta Q_1 - P_1 + \left[ \sum_{k=2}^N d_{11k} \frac{2\eta q_k \pm p_k}{4\eta^2 + \epsilon_k} \right] Q_1 \\ &\quad \pm \frac{1}{2} \eta \sum_{i,k=2}^N (U_{ik} q_i q_k + u_{ik} q_i Q_k + u_{ik} Q_i q_k) \\ &\quad \pm \frac{1}{2} \eta \sum_{i,k=2}^N (V_{ik} p_i p_k + v_{ik} p_i P_k + v_{ik} P_i p_k) \\ &\quad + \sum_{i,k=2}^N (W_{ik} q_i p_k + w_{ik} q_i P_k + w_{ik} Q_i p_k). \end{aligned} \quad (\text{A32})$$

Term  $A$  comes from the correspondence of state points used in the difference method while term  $B$  comes from the changes of center stable or unstable manifold introduced by the mass change.

\*Permanent address: Dipartimento di Fisica, Università degli Studi di Trento, I-38050 Povo, Trento, Italy.

<sup>1</sup>G. H. Vineyard, *J. Phys. Chem. Solids* **3**, 121 (1957).

<sup>2</sup>N. L. Peterson, in *Diffusion in Solids*, edited by A. S. Nowick and J. J. Burton (Academic, New York, 1975), and references therein.

<sup>3</sup>J. N. Mundy, L. W. Barr, and F. A. Smith, *Philos. Mag.* **14**, 785 (1966); J. N. Mundy, *Phys. Rev. B* **3**, 2431 (1971).

<sup>4</sup>C. P. Flynn, *Phys. Rev. Lett.* **35**, 1721 (1975).

<sup>5</sup>C. H. Bennett, in *Diffusion in Solids*, edited by A. S. Nowick and J. J. Burton (Academic, New York, 1975).

<sup>6</sup>C. H. Bennett, *Thin Solid Films* **25**, 65 (1975).

<sup>7</sup>J. N. Mundy, C. W. Tse, and W. D. McFall, *Phys. Rev. B* **13**, 2349 (1976); J. N. Mundy, H. A. Hoff, J. Pelleg, S. J. Rothman, L. J. Nowicki, and F. A. Schmidt, *ibid.* **24**, 658 (1981).

<sup>8</sup>M. J. Jackson and D. Lazarus, *Phys. Rev. B* **15**, 4644 (1977).

<sup>9</sup>C. Herzig, H. Eckeler, W. Bussmann, and D. Cardis, *J. Nucl. Mater.* **69/70**, 61 (1978); see also the review of C. Herzig and U. Kohler, *Mater. Sci. Forum* **15/18**, 301 (1987).

<sup>10</sup>G. De Lorenzi, G. Jacucci, and C. P. Flynn, *Phys. Rev. B* **30**, 5430 (1982).

<sup>11</sup>M. Toller, G. Jacucci, G. De Lorenzi, and C. P. Flynn, *Phys.*

- Rev. B **32**, 2082 (1985).
- <sup>12</sup>G. Jacucci, G. De Lorenzi, M. Marchese, C. P. Flynn, and M. Toller, Phys. Rev. B **36**, 3086 (1987).
- <sup>13</sup>J. D. Doll and A. F. Voter, Ann. Rev. Phys. Chem. (to be published).
- <sup>14</sup>A. F. Voter and J. D. Doll, J. Chem. Phys. **80**, 5832 (1984).
- <sup>15</sup>A. F. Voter and J. D. Doll, J. Chem. Phys. **82**, 80 (1985).
- <sup>16</sup>H. Frauenfelder and P. G. Wolynes, Science **229**, 337 (1985).
- <sup>17</sup>G. De Lorenzi, G. Jacucci, and C. P. Flynn, preceding paper, Phys. Rev. B **36**, 9461 (1987).
- <sup>18</sup>H. B. Huntington, M. D. Feit, and D. Lortz, Cryst. Lattice Defects **1**, 193 (1970).
- <sup>19</sup>C. P. Flynn, Mater. Sci. Forum, **15/18**, 281 (1987).
- <sup>20</sup>G. Ciccotti and G. Jacucci, Phys. Rev. Lett. **35**, 789 (1975).
- <sup>21</sup>G. Ciccotti, G. Jacucci, and I. R. McDonald, J. Stat. Phys. **21**, 1 (1979).
- <sup>22</sup>C. P. Flynn and G. Jacucci, Phys. Rev. B **25**, 6225 (1982).
- <sup>23</sup>G. Jacucci, in *Diffusion in Crystalline Solids*, edited by G. E. Murch and A. S. Nowick (Academic, New York, 1984).
- <sup>24</sup>A. F. Voter, Phys. Rev. B **34**, 6819 (1986).
- <sup>25</sup>L. Verlet, Phys. Rev. **165**, 209 (1968).